Mercury speciation and mercury isotope fractionation during ore roasting process and their implication to source identification of downstream sediment in the Wanshan mercury mining area, SW China

Runsheng Yin [a,b], Xinbin Feng [a,*], Jianxu Wang [a,b], Ping Li [a], Jinling Liu [a,b], Ying Zhang [a,c], Jiubin Chen [a], Lirong Zheng [d], Tiandou Hu [d]

[a] State Key Laboratory of Environmental Geochemistry, Institute of Geochemistry, Chinese Academy of Sciences, Guiyang 550002, China
[b] Graduate University of Chinese Academy of Sciences, Beijing 100049, China
[c] State Key Laboratory of Ore Deposit Geochemistry, Institute of Geochemistry, Chinese Academy of Sciences, Guiyang 550002, China
[d] Beijing Synchrotron Radiation Facility, Institute of High Energy Physics, Chinese Academy of Sciences, Beijing 100049, China

ARTICLE INFO

ABSTRACT

The environment of Guizhou province of SW China is in part significantly impacted by mercury (Hg) mining activities. The exploitation and processing of Hg-bearing ore in the past have led to multiple sources of Hg contamination, including unprocessed ores and Hg waste calcines and liquid elemental Hg, making source control strategies difficult and expensive to implement. In this study, initially extended X-ray absorption fine structure (EXAFS) spectroscopy was used to determine the Hg species and to estimate the relative proportions of these species present in Hg-bearing wastes from the Wanshan Hg mine (WSMM) of the eastern Guizhou province. The results showed that cinnabar is the dominant Hg species in the unroasted ore samples, while the most prevalent Hg compounds in mine waste calcine is in the following order: meta-cinnabar, cinnabar and mercuric chloride. Our study demonstrated that mass dependent fractionation of Hg isotopes may occur during transformation of cinnabar to by-products (such as meta-cinnabar and mercuric chloride) by the roasting process. Hg stable isotope analysis of unroasted Hg ores and Hg waste calcines showed that Hg waste calcines ($0.08 \pm 0.20‰$, $2\acute{o}$, n = 11) were enriched by ~0.80‰ in δ^{202}Hg values compared to the unroasted Hg ores ($-0.74 \pm 0.11‰$, $2\acute{o}$, n = 14). Finally, using a combined triple mixing model, the source attribution of the downstream sediment in WSMM was estimated. Our study suggested that the Hg isotope could be a useful tool to trace and quantify the source of Hg in the environment.

1. Introduction

Mercury (Hg) is a naturally occurring element that poses considerable health risks to humans (NRC, 2000). Elevated concentrations of Hg can be found in Hg mining-impacted regions, resulting in widespread contamination of the immediate mining site and the surrounding environment (Kim et al., 2004). Hg contamination is particularly prevalent in Guizhou province, SW China. There are at least 12 large (with Hg resource of 2000–10,000 t) and one super-large (with Hg resource > 10,000 t) Hg mines present in this province (SWSNANE, 2003; Feng and Qiu, 2008). In Guizhou, although large-scale Hg mining activities have been officially suspended since the beginning of this century, nevertheless the environmental impacts of Hg mining operations are chronic. Large volumes of Hg-bearing waste rocks and roasted calcines are present at these mine sites with residual levels of Hg ranging in concentration from < 100 to several 1000 μg g^{-1}, which causes serious pollution to soil/sediment (Zhang et al., 2004; Qiu et al., 2005), water (Zhang et al., 2010), and agricultural crops (Horvat et al., 2003; Feng et al., 2008; Qiu et al., 2008) in the surroundings.

The speciation of Hg in Hg mine wastes is a critical factor in determining its mobility, reactivity, and potential bioavailability in the mining regions (Kim et al., 2000). Since different Hg species possess varying degrees of solubility, the particular species present and their relative proportions in an Hg-contaminated source can greatly influence the release and transport of Hg. Therefore, knowing Hg speciation in mine wastes can provide insights about the processes of Hg release and distribution in a specific site. Furthermore, extended X-ray absorption fine structure (EXAFS) spectroscopy is a powerful technique to investigate chemical speciation (Huggins et al., 2000). This non-destructive technique is one of the few direct techniques available for determining Hg speciation in relatively low-concentration samples such as mine wastes (Kim et al., 2004).

Recent development of analytical methods for heaviest isotopes has spurred interest in using stable isotopes of Hg to identify sources and to determine fates of Hg in the environment (Blum and Bergquist, 2007; Koster van Groos et al., 2007; Yin et al., 2010a). A large variation

* Corresponding author. Tel.: +86 851 5891356; fax: +86 851 5891609.
E-mail address: fengxinbin@vip.skleg.cn (X. Feng).

in Hg isotope compositions has been reported in-between a variety of environmental samples including Hg-ores (Hintelmann and Lu, 2003; Smith et al., 2005, 2008; Stetson et al., 2009), hydrothermal emissions (Smith et al., 2008; Sherman et al., 2009; Zambardi et al., 2009), Hg mine waste (Stetson et al., 2009), sediments (Foucher and Hintelmann, 2006; Foucher et al., 2009; Gehrke et al., 2009; Feng et al., 2010; Liu et al., 2011), coals and soils (Biswas et al., 2008; Lefticariu et al., 2011), and fish (Bergquist and Blum, 2007; Jackson et al., 2008; Laffont et al., 2009; Perrot et al., 2010). The above cited studies have unequivocally demonstrated that variations in the Hg isotopic signature could be used in the future as tracers to distinguish between Hg sources and important chemical transformation processes in the environment.

In this paper, a case study is presented that was carried out in the Wanshan mercury mining area (WSMM), Guizhou Province, China. The objectives of this study are 1) to determine the speciation of Hg in unroasted ore and calcine samples collected from WSMM using the EXAFS spectroscopy method; 2) to determine whether Hg isotope compositions can be used to distinguish Hg sources (e.g. unprocessed Hg-ores, mine-waste calcines) at the mining sites; and 3) to investigate the Hg sources of Hg in downstream sediment in WSMM.

2. Materials and methods

2.1. Study areas and sampling

A map encompassing the WSMM study area is given in Fig. 1. WSMM, also known as the "Mercury Capital" in China, is located in the eastern part of Guizhou province, China. In this area, Hg mining activities have been documented for more than 3000 years (Feng and Qiu,

2008). Hg ores had been intensively extracted from WSMM during the past 50 years. Approximately 125.8 million tons of calcines had been dispersed into the adjacent ecosystems before it was officially closed in 2001(Zhang et al., 2004; Qiu et al., 2005). Specifically, one of the five major river valleys in the area, the Dashuixi (DSX) River was studied due to significant amount of discarded tailings (at Wukeng, WK) present at the headwater. We collected downstream sediment samples at WSMM in October 2008. Sediment samples collected were composed of surface sediments (0–2 cm) of the DSX River and were a composite of at least 4 sub-samples, for increased spatial resolution. The sampling locations of the river sediment are presented in Fig. 1. On that occasion, unroasted Hg ore and Hg waste calcine samples were also collected. During our sampling campaign, all collected samples were stored in sealed polyethylene bags to avoid cross contamination and were then shipped to the laboratory as soon as possible after collection. In the laboratory, after homogenization, milling and riffling, the samples were ground to sub-minus 150 mesh ($\leq$106 μm) and subsequently sealed in polyethylene bags prior to total Hg concentration (HgT), EXAFS and Hg isotopic analysis.

2.2. Total mercury analysis

Total mercury (HgT) concentrations in sediments, unroasted Hg ore and Hg waste calcines were analyzed using Lumex RA 915$^+$ Hg analyzer (Lumex Ltd., Russia) following the method reported by Luis et al. (2007). The detection limit for HgT was 0.5 ng g^{-1}. All the samples were analyzed in triplicate. Quality control for the Hg analysis was addressed with certified reference materials (GBW 07305, GBW 07405), with an average recovery of 94%.
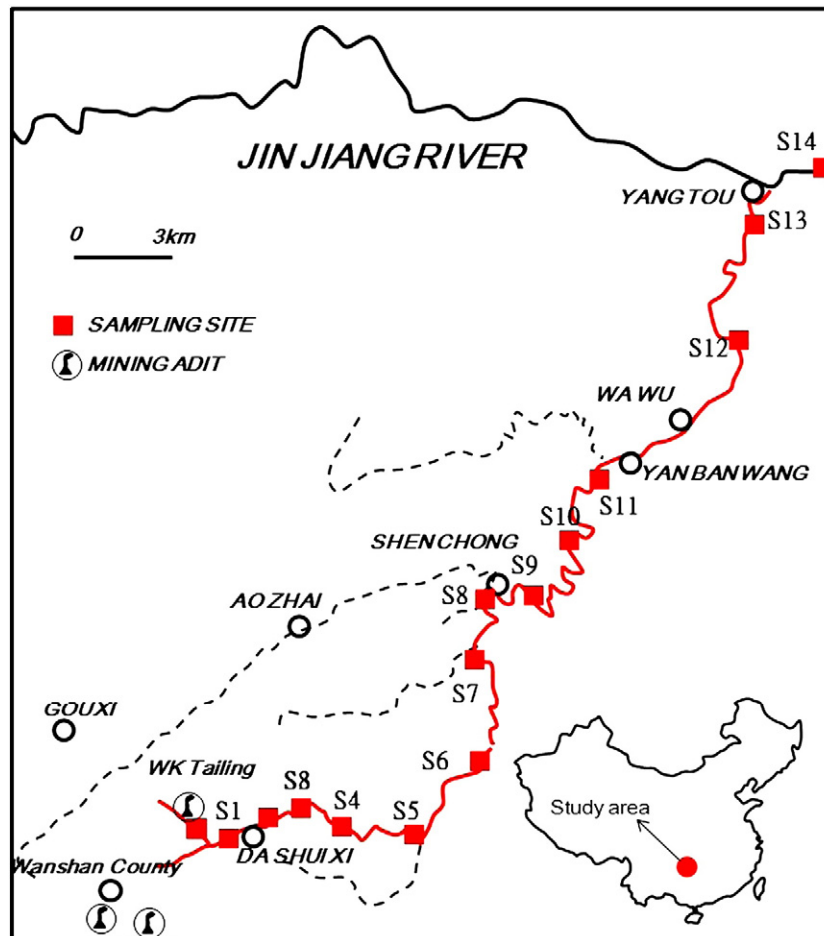

Fig. 1. Overview map of the study area in WSMM of Guizhou Province, China.

2.3. Mercury speciation protocol

Two composite samples of unroasted Hg ores (n = 14) and waste calcines (n = 11) in WSMM were analyzed by EXAFS. Mercury LIII-edge X-ray absorption spectra were collected at the EXAFS station of Beijing Synchrotron Radiation Facility (BSRF). Mercury LIII-edge (12.28 keV) X-ray absorption spectra were collected at the 1W1B beamline of the Beijing Synchrotron Radiation Facility (Beijing, China). Cinnabar (α-HgS), meta-cinnabar (β-HgS), mercuric chloride ($HgCl_2$), montroydite (HgO), and mercuric sulfate ($HgSO_4$), the possible components of Hg in the measured samples, were chosen as reference materials, and their XAFS spectra were also measured as shown in Fig. 2. We did not measure the elemental Hg in our EXAFS study. Elemental Hg^0 is a semi-volatile species with a vapor pressure of 0.18 Pa at 20 °C (Schroeder and Munthe, 1998). Several studies demonstrated the existence of a minor proportion of Hg^0 in the ore and Hg calcines in other Hg mines. However, besides some individual samples, the fraction of Hg^0 in most samples usually represented <0.1% of the total Hg (Gray et al., 2000, 2006). Considering the roasting temperatures of 700–850 °C associated with Hg^0 production operations in WMMA (Zhao and Wang, 1999), the mobility of this species will be greatly enhanced during retorting. Hence, we would not expect to find significant amounts of elemental Hg^0 in the fine powder of Hg ore and Hg waste calcine. An EXAFS study by Kim et al. (2004) did not show a substantial amount of liquid Hg^0 in either Hg ore or Hg waste calcines collected in several Hg mines in the California Coast Range Hg mineral belt. Data normalization (baseline and background corrections) together with cubic spline interpolation, Fourier transformation and EXAFS fitting were performed using the program WinXAS v 3.1(Ressler, 1998). To acquire a convincing measure of components and their relative proportions, a linear combination fitting (LCF) X-ray absorption near edge structure spectrometry of the adsorption samples using reference components was executed through the Athena program in the IFEFFIT computer package (Newville, 2001). More details of the method were described in Lv et al. (2012).

2.4. MC-ICP-MS measurement protocol

Hg isotopic ratios were determined by MC-ICP-MS using a Nu-Plasma mass spectrometer equipped with twelve Faraday cups (Nu Instruments,
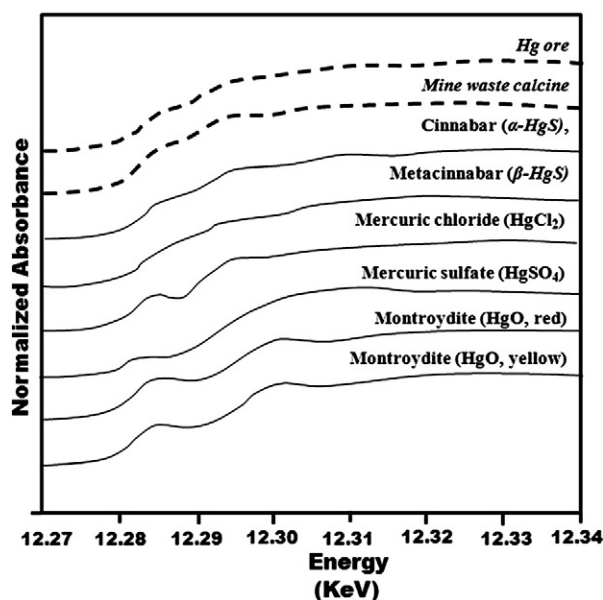

Fig. 2. Normalized absorbance curves of mercury K-edge XANES spectra of the reference compounds and unknown samples.

Great Britain) at the State Key Laboratory of Environmental Geochemistry, Institute of Geochemistry, Chinese Academy of Sciences, China. A continuous flow cold-vapor generation system (CV) (HGX-200, CETAC U.S.) was coupled with an Apex-Q desolvation unit (Elemental Scientific Inc., U.S.) for Hg and Tl introduction, respectively. A more detailed description of the overall instrumental setup, as well as the parameters and analytical conditions used throughout this study can be found in Yin et al. (2010b).

Hg isotopic variations are reported here in delta notation in units of per mil (‰) and referenced to the NIST SRM 3133 Hg standard (analyzed before and after each sample) and using the following equation:

$$\delta^{xxx}Hg(‰) = \left\{ \left({^{xxx}Hg}/{^{198}Hg}_{sample} \right) / \left({^{xxx}Hg}/{^{198}Hg}_{NISTSRM3133} \right) - 1 \right\} \times 1000. \tag{1}$$

Mass independent fractionation (MIF) of Hg isotopes is calculated using the "capital delta" notation, $\Delta^{xxx}Hg$ (‰), which is defined as the difference between the measured $\delta^{xxx}Hg$ values and the predicted $\delta^{xxx}Hg$ values from MDF, following Eqs. (2) and (3) reported by Blum and Bergquist (2007).

$$\Delta^{201}Hg \approx \delta^{201}Hg - \left(\delta^{202}Hg * 0.752 \right) \tag{2}$$

$$\Delta^{199}Hg \approx \delta^{199}Hg - \left(\delta^{202}Hg * 0.252 \right) \tag{3}$$

Reproducibility of the isotopic data was assessed by measuring replicate sample digests (typically n = 2). We also analyzed the UM-Almadén as a secondary standard (once in every 10 samples) in the analytical season. Hg in UM-Almadén was measured in the same way as the other samples in each analytical session. The overall average and uncertainty of $\delta^{202}Hg$ was -0.53 ± 0.10‰ (2ó, n = 9), of $\Delta^{201}Hg$ was 0.01 ± 0.08‰ (2ó, n = 9) and of $\Delta^{199}Hg$ was -0.01 ± 0.08‰ (2ó, n = 9) for all UM-Almadén measurements, which agrees well with data reported in Blum and Bergquist (2007). Uncertainties reported in the figures and table of this paper correspond to the larger value of either 1) the measurement uncertainty of replicate digests, or 2) the uncertainty of repeated measurements of the same digest at different analysis sessions. In cases where the corresponding calculated 2ó was smaller than that derived from the replicate analyses of the reference material of UM-Almadén, the uncertainty associated to UM-Almadén was used instead.

Based on the HgT content measured in Section 2.2, all samples were weighted and digested with a fresh mixture of HNO_3–HCl (1:3, v/v) in a water bath (95 °C), and were diluted to yield a final Hg concentration of at least 5 ng mL^{-1} before MC-ICP-MS analysis. HgT concentrations of digest solutions were also estimated by MC-ICP-MS using ^{202}Hg signals. The differences between the HgT measured by Lumex RA 915$^+$ and MC-ICP-MS were <11%.

3. Results and discussion

3.1. Effect of ore roasting on Hg speciation

Based on the linear fitting analysis of XAFS spectra recorded for unroasted Hg ore and Hg waste calcine sample, we were able to acquire a robust measurement of the components and their relative proportions. As shown in Fig. 3, our data indicate that α-HgS is the dominant Hg species in the unroasted waste ore samples ($99 \pm 0.5\%$, 2ó, n = 3) with only a minor proportion of β-HgS ($1 \pm 0.5\%$, 2ó, n = 3). However, the dominant components in the mine waste calcine are β-HgS ($52 \pm 0.5\%$, 2ó, n = 3), α-HgS ($42 \pm 0.5\%$, 2ó, n = 3) and $HgCl_2$ ($6 \pm 0.5\%$, 2ó, n = 3). The identification of the relevant Hg species present is consistent with the field studies that cinnabar is the primary ore mineral in Hg deposits in WSMM (Feng and Qiu, 2008). The geological origin of WSMM
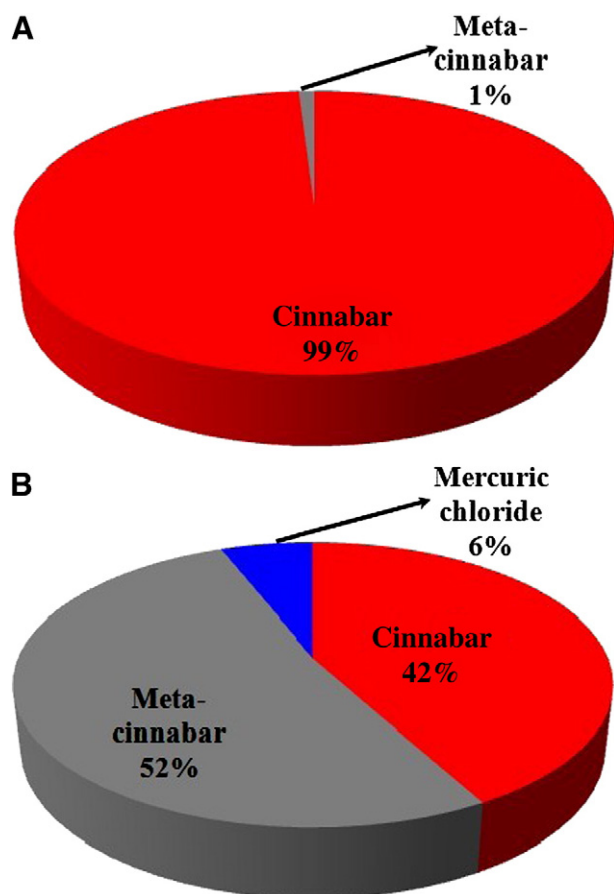
A

B

Fig. 3. Composition of Hg species in unroasted Hg ore (A) and Hg waste calcine (B) in WSMM (based on the linear fitting results of the EXAFS data).

is of silica-carbonate deposit type, in which Hg-sulfide in the form of α-HgS is dominant (Chen and Sun, 1991).

As shown in Fig. 3, the high proportion of β-HgS in mine waste calcine supported the reconstructive phase transformation of α-HgS to β-HgS during the calcining process. In an EXAFS study by Kim et al. (2004), Hg phases and fractions of these phases presented in Hg mine wastes from selected Hg mines in California and Nevada were investigated. Their data indicated that Hg waste calcines contained high proportions of β-HgS while the main Hg-containing phase in unroasted ore samples consists of α-HgS. The presence of mercuric chloride ($6 \pm 0.5\%$, 2ό, n = 3) in the WSMM calcine sample indicates that the conversion of α-HgS to elemental Hg^0 during retorting to some extent yield by-products (Kim et al., 2004).

3.2. Fractionation of mercury isotope compositions during ore roasting

The Hg isotope composition of unroasted Hg ores and Hg waste calcines in WSMM is given in Table 1. As shown in Fig. 4, the total range of $\delta^{202}Hg$ for the multiple samples of Hg ores was confined in the range from −0.56 to −0.92‰, with a mean value of −0.74 ± 0.11‰ (2ό, n = 14). No statistically significant MIF ($\Delta^{199}Hg$~0‰) was observed in any of the Hg ore samples analyzed as shown in Table 1. Smith et al. (2005) reported large Hg isotope fractionation (>5‰ in $\delta^{202}Hg$ values) in Hg ores in two epithermal mineral deposits in the national and Ivanhoe mining districts of northern Nevada in the U.S. They demonstrated that the large MDF of Hg isotopes probably resulted from the combination of boiling of the hydrothermal fluid, oxidation near the surface, and kinetic effects associated with mineral precipitation. Similarly, Smith et al. (2008) investigated the isotopic composition of Hg in rocks, ore deposits, and active spring deposits from the California Coast Ranges. The large

variation of $\delta^{202}Hg$ (ranged from −3.88 to 1.61‰) in their study indicated that boiling of hydrothermal fluids, separation of an Hg-bearing CO_2 vapor or reduction and volatilization of Hg^0 in the near-surface environment are likely the most important processes causing the MDF in the hydrothermal system. However, Smith et al. (2008) also demonstrated that the release of Hg from its source rocks into hydrothermal solutions and during transport and concentration of Hg in deposits would not cause significant MDF. Hintelmann and Lu (2003) also reported large variations of $\delta^{202}Hg$ (−1.73 to 1.33‰) in Hg ore samples collected from several Hg deposits worldwide. Although the above studies reported a wide variation in $\delta^{202}Hg$ compositions for various Hg deposits worldwide, our Hg isotopic analysis of numerous Hg ore samples indicates that Hg ore at WSMM exhibits an isotopically narrow range of $\delta^{202}Hg$ composition of −0.74 ± 0.11‰ (2ό, n = 14). Similarly, Stetson et al. (2009) also reported a relative narrow range of Hg isotopes from two large Hg mining districts [McDermitt Mine ($\delta^{202}Hg$ = −0.60 ± 0.20‰, 2ό, n = 11) and Terlingua Mine ($\delta^{202}Hg$ = −1.66 ± 0.12‰, 2ό, n = 3)] in the U.S.

As shown in Fig. 4, $\delta^{202}Hg$ of WSMM calcines varied from −0.20‰ to 0.53‰, with a mean value of 0.08 ± 0.20‰ (2ό, n = 11) being isotopically heavier than the unroasted Hg ores (−0.74 ± 0.11‰, 2ό, n = 14). Hence, an Hg isotopic fractionation of ~0.80‰ in $\delta^{202}Hg$ values during Hg retorting process is implied. MIF in Hg waste calcines ($\Delta^{199}Hg$ = −0.00 ± 0.03‰, 2ό, n = 11) is statistically insignificant. Our study is in good agreement with previous studies (Stetson et al., 2009; Sonke et al., 2010; Gehrke et al., 2011). Stetson et al. (2009) reported significant MDF of Hg isotopes during retorting in two Hg mining districts in Terlingua (Texas) and McDermitt (Nevada) in the U.S. Their study indicated that calcines were enriched by ~1.90‰ (in Terlingua) and ~0.10‰ (in McDermitt) in $\delta^{202}Hg$ values compared to the cinnabar samples. Gehrke et al. (2011) presented the Hg isotope composition of Hg calcines from the New Idria Hg mine, U.S. They found that Hg waste calcines were enriched by ~0.40‰ in $\delta^{202}Hg$ values compared to the unroasted Hg ores. Sonke et al. (2010) demonstrated MDF of Hg isotopes during the smelting of sphalerite concentrates in high temperature pyrometallurgical conditions, and the Zn slags ($\delta^{202}Hg$ = −0.24 ± 0.71‰, 2ό, n = 4) appeared to be enriched in heavy Hg isotopes compared to that of sphalerite concentrates ($\delta^{202}Hg$ = −0.65 ± 1.33‰, 2ό, n = 4).

In WSMM, Hg ores (mainly as α-HgS) were crushed and then roasted in a calcinator at a temperature range of 700–850 °C (Zhao and Wang, 1999). During the roasting process, the product Hg^0 readily distils from the calcinator due to its relatively low boiling point. The operations of Hg smelting, roasting and retorting are combined to be essentially included in a single reactor. This process produces calcines and elemental Hg^0. According to our study, the average HgT in unroasted Hg ore samples is 11,477 $\mu g\,g^{-1}$, which is substantially higher than that in calcines (57 $\mu g\,g^{-1}$), suggesting that Hg in calcine represents <0.05% of the total Hg in Hg ores. Even at an assumed substantial difference of 8.0‰ in $\delta^{202}Hg$ values between Hg waste calcines and unroasted ore samples, an insignificant difference of <0.05‰ in $\delta^{202}Hg$ values is expected to be observed between the released Hg^0 and the unroasted ore samples. Since 8.0‰ corresponds to the largest deviation in $\delta^{202}Hg$ observed so far in natural samples, we would not whatsoever be able to observe significant Hg isotope composition fractionation between Hg^0 and Hg ores.

Biogeochemical processes involving Hg, such as microbial reduction (Kritee et al., 2007, 2008), photo reduction (Bergquist and Blum, 2007; Yang and Sturgeon, 2009; Zheng and Hintelmann, 2009), evasion processes (Zheng et al., 2007) and evaporation (Estrade et al., 2009) lead to enrichment of heavy Hg isotopes in the residual phase. In WSMM, the Hg remaining in the calcines might be isotopically heavier than the parent material depending on the fractionation factor for reduction of cinnabar to elemental Hg. Isotope fractionation of Zn isotopes during a metallurgical process has been investigated by several studies (Sonke et al., 2008; Mattielli et al., 2009). Sonke et al. (2008) demonstrated that slag residues produced by metallurgical activities were characterized by enrichment in heavy Zn isotopes compared to that of the initial ores. Mattielli et al. (2009) suggested that the volatilization/condensation

Table 1
Total mercury concentration and mercury isotope composition for samples of DSX downstream sediments and UM-Almadén (n = 9).

Sample ID	Distance (km)	HgT (µg/g)	$\delta^{199}Hg$ ‰	2SD ‰	$\delta^{200}Hg$ ‰	2SD ‰	$\delta^{201}Hg$ ‰	2SD ‰	$\delta^{202}Hg$ ‰	2SD ‰	$\Delta^{199}Hg$ ‰	2SD ‰	$\Delta^{201}Hg$ ‰	2SD ‰	$\Delta^{200}Hg$ ‰	2SD ‰
DSX River downstream sediments																
S1	0.5	25	0.05	0.01	0.06	0.01	0.12	0.04	0.12	0.02	0.02	0.06	0.03	0.02	0.03	0.01
S2	2.6	85	0.00	0.08	0.11	0.10	0.13	0.07	0.21	0.19	−0.05	0.03	−0.03	0.07	0.07	0.01
S3	3.7	82	0.01	0.11	0.03	0.08	0.02	0.15	0.05	0.16	0.03	0.07	−0.02	0.03	0.08	0.05
S4	4.9	53	0.05	0.04	0.06	0.09	0.10	0.15	0.11	0.16	0.02	0.02	0.02	0.03	0.05	0.05
S5	6.3	18	−0.01	0.02	0.02	0.02	0.05	0.08	0.04	0.08	−0.02	0.04	0.02	0.02	−0.04	0.04
S6	9.5	19	0.00	0.04	−0.05	0.09	−0.05	0.15	−0.09	0.16	0.02	0.02	0.02	0.03	0.02	0.03
S7	13	12	−0.05	0.02	−0.08	0.02	−0.13	0.01	−0.15	0.08	−0.01	0.02	−0.02	0.01	0.05	0.03
S8	15	10	−0.08	0.01	−0.17	0.02	−0.27	0.01	−0.34	0.02	0.01	0.04	−0.01	0.01	0.06	0.01
S9	17	15	−0.07	0.01	−0.23	0.08	−0.32	0.15	−0.45	0.16	0.04	0.03	0.02	0.03	0.03	0.04
S10	20	4	−0.13	0.01	−0.33	0.02	−0.45	0.03	−0.65	0.02	0.03	0.03	0.04	0.01	0.01	0.05
S11	23	13	−0.14	0.02	−0.29	0.02	−0.46	0.08	−0.57	0.08	0.00	0.04	−0.03	0.02	0.06	0.04
S12	29	2	−0.11	0.02	−0.27	0.01	−0.39	0.06	−0.53	0.08	0.02	0.04	0.01	0.02	0.07	0.04
S13	33	1	−0.18	0.01	−0.42	0.02	−0.65	0.03	−0.83	0.02	0.03	0.01	−0.03	0.01	0.06	0.03
S14	34	1	−0.20	0.05	−0.40	0.08	−0.60	0.12	−0.79	0.16	0.00	0.01	−0.01	0.00	0.03	0.02
WSMM Hg ores																
Cin.-WS-1		10,600	−0.16	0.01	−0.38	0.01	−0.59	0.01	−0.75	0.03	0.03	0.01	−0.03	0.03	0.08	0.02
Cin.-WS-2		13,500	−0.25	0.01	−0.46	0.02	−0.66	0.03	−0.92	0.05	−0.02	0.03	0.03	0.01	0.08	0.02
Cin.-WS-3		9900	−0.16	0.05	−0.30	0.07	−0.47	0.10	−0.60	0.15	−0.01	0.01	−0.02	0.01	−0.01	0.02
Cin.-WS-4		26,100	−0.17	0.06	−0.36	0.10	−0.56	0.17	−0.71	0.20	0.01	0.01	−0.03	0.02	−0.04	0.02
Cin.-WS-5		11,700	−0.16	0.04	−0.33	0.01	−0.50	0.05	−0.66	0.01	0.01	0.04	0.00	0.04	0.00	0.02
Cin.-WS-6		9800	−0.24	0.04	−0.45	0.01	−0.65	0.05	−0.89	0.01	−0.02	0.04	0.02	0.04	0.06	0.05
Cin.-WS-7		46,000	−0.21	0.04	−0.41	0.01	−0.59	0.05	−0.82	0.01	0.00	0.04	0.03	0.04	0.00	0.02
Cin.-WS-9		3400	−0.15	0.04	−0.40	0.01	−0.56	0.02	−0.80	0.02	0.05	0.04	0.04	0.03	0.06	0.03
Cin.-WS-10		2400	−0.18	0.04	−0.40	0.04	−0.55	0.04	−0.79	0.09	0.02	0.02	0.04	0.03	0.06	0.02
Cin.-WS-11		3500	−0.17	0.08	−0.35	0.14	−0.52	0.21	−0.70	0.27	0.01	0.01	0.01	0.01	−0.02	0.02
Cin.-WS-12		4100	−0.12	0.01	−0.28	0.02	−0.41	0.05	−0.56	0.03	0.02	0.04	0.01	0.02	−0.04	0.02
Cin.-WS-13		2700	−0.18	0.10	−0.39	0.18	−0.62	0.31	−0.78	0.38	0.02	0.01	−0.03	0.02	0.04	0.02
Cin.-WS-14		5500	−0.16	0.01	−0.34	0.03	−0.53	0.05	−0.68	0.05	0.01	0.04	−0.02	0.02	0.04	0.03
WSMM Hg mine waste calcines																
Cal.-WS-1		49	−0.01	0.02	0.06	0.02	0.08	0.13	0.11	0.08	−0.04	0.04	0.00	0.07	0.05	0.02
Cal.-WS-2		63	−0.03	0.08	−0.06	0.04	−0.09	0.09	−0.12	0.08	0.00	0.06	0.00	0.03	−0.03	0.03
Cal.-WS-3		57	0.05	0.01	0.06	0.01	0.10	0.01	0.11	0.01	0.02	0.01	0.02	0.02	0.04	0.04
Cal.-WS-4		47	0.08	0.01	0.04	0.01	0.08	0.01	0.07	0.01	0.06	0.01	0.03	0.03	−0.03	0.03
Cal.-WS-5		63	−0.06	0.01	−0.08	0.02	−0.13	0.02	−0.16	0.01	−0.02	0.02	−0.01	0.02	0.05	0.03
Cal.-WS-6		73	−0.04	0.01	−0.10	0.02	−0.14	0.01	−0.20	0.01	0.01	0.02	0.01	0.01	0.00	0.05
Cal.-WS-7		61	0.05	0.02	0.08	0.01	0.13	0.04	0.16	0.03	0.01	0.01	0.01	0.02	−0.04	0.03
Cal.-WS-8		68	0.13	0.01	0.27	0.02	0.43	0.04	0.53	0.04	0.00	0.04	0.03	0.01	0.05	0.01
Cal.-WS-9		40	0.06	0.01	0.08	0.02	0.13	0.02	0.16	0.01	0.02	0.01	0.01	0.01	0.05	0.03
Cal.-WS-10		59	−0.02	0.02	−0.01	0.01	−0.06	0.06	−0.01	0.04	−0.02	0.03	−0.05	0.03	0.01	0.02
Cal.-WS-11		46	0.06	0.02	0.10	0.02	0.11	0.05	0.20	0.05	0.01	0.03	−0.04	0.01	−0.03	0.02
Standard materials																
UM-Almadén			−0.14	0.08	−0.27	0.08	−0.39	0.09	−0.53	0.10	−0.01	0.08	0.01	0.08	−0.04	0.08

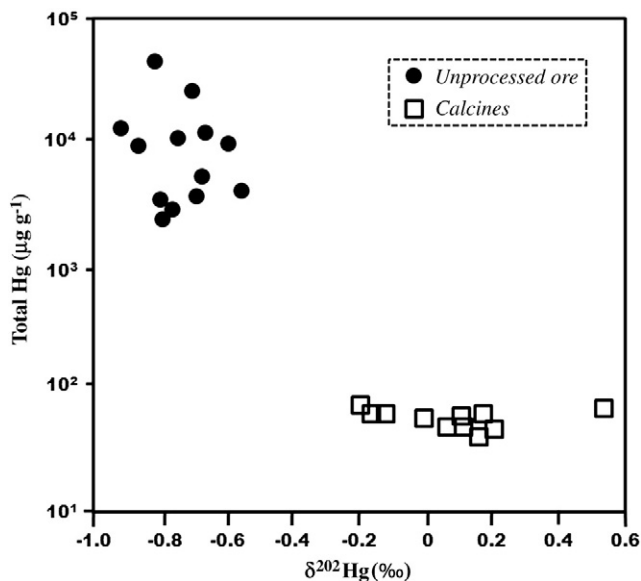**Fig. 4.** Total Hg (HgT) concentrations and Hg isotope variations during Hg roasting process. Plot of $\delta^{202}Hg$ (in ‰) vs HgT (in µg g^{-1}, log scale).

of Zn in high temperature condition during Zn smelting may induce isotopic fractionation. For Hg, it has been demonstrated that the evaporation (22–100 °C) of liquid Hg^0 yields residual Hg^0 with higher $\delta^{202}Hg$ values than that of Hg^0 vapor distilled (Estrade et al., 2009).

The reconstructive phase transformation of α-HgS to Hg by-product species (e.g. β-HgS and HgCl$_2$) during the calcining process in WSMM may also yield Hg calcines with higher $\delta^{202}Hg$ values than the parent Hg ores. Stetson et al. (2009) demonstrated that the newly formed Hg species during retorting are expected to be enriched in the heavier Hg isotopes. β-HgS is the isometric form of α-HgS (Kullerud, 1965). Foucher et al. (2009) have reported the presence of isotopically heavier β-HgS ($\delta^{202}Hg = 0.23$‰) than α-HgS ($\delta^{202}Hg = -0.26$‰) in the Idrija Hg mine, Slovenia. Stetson et al. (2009) demonstrated heavier Hg isotope compositions in β-HgS ($\delta^{202}Hg = -0.07$, n = 1) than α-HgS ($\delta^{202}Hg = -1.66 \pm 0.12$‰, 2ó, n = 3) in Terlingua Hg deposits in Texas, U.S. The HgCl$_2$ formed through the conversion of α-HgS to elemental Hg^0 during retorting might be enriched in heavier Hg isotopes. Theoretical calculations by Schauble (2007) suggested that the heavier isotopes of Hg will be preferentially partitioned into the oxidized Hg species compared to the elemental Hg^0. In a study by Stetson et al. (2009), the $\delta^{202}Hg$ of by-product HgCl$_2$ ($\delta^{202}Hg = -1.40 \pm 0.92$‰, 2ó, n = 2) collected from the Terlingua Hg mine (U.S.) exhibited a tendency to be isotopically heavier than that of α-HgS ($\delta^{202}Hg = -1.66 \pm 0.12$‰, 2ó, n = 3).

Due to the difficulty in selecting the Hg by-products in calcines, it is impossible for us to measure the isotope compositions of individual Hg compounds (e.g. α-HgS, β-HgS and HgCl$_2$) in calcines. Although there is still the possibility that the cinnabar remaining after processing is isotopically different than the ore, if we assumed that the δ^{202}Hg value of α-HgS in the Hg waste calcine is the same as that in the unroasted Hg ore (δ^{202}Hg = −0.74 ± 0.11‰, 2ό, n = 14), we can roughly estimate the δ^{202}Hg of the by-product based on Eqs. (4) and (5):

$$F_{byp.} \times \delta^{202}Hg_{byp.} + \left(1 - F_{byp.}\right) \times \delta^{202}Hg_{\alpha-HgS} = \delta^{202}Hg_{calcine} \quad (4)$$

$$\delta^{202}Hg_{byp.} = \left(\delta^{202}Hg_{calcine} - \delta^{202}Hg_{\alpha-HgS} + F_{byp.} \times \delta^{202}Hg_{\alpha-HgS}\right) / \left(F_{byp.}\right) \quad (5)$$

where δ^{202}Hg$_{byp.}$ and δ^{202}Hg$_{\alpha\text{-}HgS}$ refer to the δ^{202}Hg value of Hg by-products and α-HgS in the calcine sample respectively; F$_{byp.}$ refers to the fraction of Hg by-products in Hg waste calcines; δ^{202}Hg$_{calcine}$ refers to the average δ^{202}Hg value of the Hg waste calcines (0.08 ± 0.20‰, 2ό, n = 11). As mentioned in Section 3.1, F$_{byp.}$ accounted for 60% (52% for β-HgS and 8% for HgCl$_2$) of the HgT in Hg waste calcines. Based on Eqs. (4) and (5), the δ^{202}Hg of the by-product is estimated to be ~0.63‰.

3.3. Tracing sources of Hg in stream sediments using mercury isotope compositions

As shown in Fig. 5, HgT content in sediments decreases from 85 to 1.0 μg g^{-1} over a distance of more than 34 km along the DSX River. The δ^{202}Hg values for DSX sediments vary from −0.83‰ to 0.21‰. No statistically significant MIF was observed as shown in Table 1. So far, data from the available literature demonstrated that the reduction processes and evasion of Hg from river basins have insignificant influence on the sediment Hg isotope composition signature (Foucher et al., 2009; Liu et al., 2011). The major processes known to induce MIF are photo-reactions of Hg in aqueous phase (Bergquist and Blum, 2007; Bergquist et al., 2011). Given the highly elevated Hg concentrations in the downstream sediments of WSMM, photochemical processes would not significantly influence the Hg isotope composition of sediments and therefore we would not expect a detectable MIF in this large Hg pool. Hence, the distinct Hg isotope signatures observed from sediments of DSX may imply that the contribution from other sources is dominating.

The geogenic baseline of Hg in soils/sediments in the area has previously been established (Hua and Cui, 1994; Qiu et al., 2005). Qiu et al. (2005) demonstrated that the local geogenic baseline of Hg in soils is

Fig. 5. Spatial distribution of δ^{202}Hg (‰) and HgT (μg g^{-1}) in sediment samples from the DSX River.

0.72 ± 0.44 μg g^{-1} (2ό, n = 6), which is similar to that reported for host rocks (0.35 μg g^{-1}) (Hua and Cui, 1994). For the DSX River transect, the samples with the lowest Hg content (~1 μg g^{-1}), which correspond to the sites at the junction of the DSX and Jinjiang River (e.g. S13 and S14), are indicative of the Hg geogenic baseline in the WSMM area (cf. Figs. 1 and 5). Compared to the uncontaminated soils, the geogenic background of Hg in the WSMM area is indeed elevated. Previous studies demonstrated elevated HgT levels in sediments and paddy soils along the DSX River basin, which is being attributed to erosion of Hg-rich particles during flood episodes (Horvat et al., 2003; Zhang et al., 2004; Qiu et al., 2005). The sediment samples in the downstream of DSX River (S13, S14) appeared to have the same Hg isotopic signature with the unroasted Hg ores, suggesting a wide spread contamination of Hg in the area derived from the unroasted ore.

In the upstream part of DSX (0–15 km), seven samples (S1–S7) displayed concentrations between 12 and 85 μg g^{-1}. Furthermore, δ^{202}Hg of the seven sediments (0.04 ± 0.12‰, 2ό, n = 7) compares favorably with that of Hg waste calcines (0.08 ± 0.20‰, 2ό, n = 11), suggesting that Hg derived from calcines constitutes the major source here. As indicated in Fig. 1, due to large-scale mining, large quantities of calcines and gangues (WK tailing) were discarded at the headwater of DSX River. HgT content in Hg waste calcines was clearly elevated in a range up to 59 μg g^{-1}, which in-turn implies that calcines and gangues are the primary Hg contamination sources to this part of the DSX River. Zhang et al. (2004) investigated Hg and several geochemical parameters in mine-waste calcines, stream sediments and surface waters in the DSX River basin. They reported that the drainage flowing out of the calcine piles had an elevated HgT concentration of 300–1900 ng L^{-1} and alkaline pH values of 10.6–11.8. They also demonstrated that the dominant mineral in downstream sediment is calcite, which indicated that the calcine pile is an important Hg source. Similarly, Zhang et al. (2010) investigated the spatial patterns of HgT and particulate Hg (HgP) species in DSX River, indicating that the highest HgT content in water samples was confined within a distance of 100–500 m downstream. Furthermore, a significant decrease in HgT content was observed at a distance of 6–8 km from the headwater. Hg in the water samples was essentially associated with particulate matter indicating the impact of erosion from waste piles (Zhang et al., 2010).

Fig. 6 displays a plot of the Hg isotopic composition (δ^{202}Hg) of the sediments versus the reciprocal of HgT concentration. The data points are interpreted as the result of a triple mixing of three sources representing (1) the geogenic background source, (2) the Hg calcine source, and (3) the unroasted Hg ore source. Notably, all three sources are without MIF. Based on Fig. 6, a triple mixing model was conducted to evaluate the relative fractions of three sources in DSX sediment using Eqs. (6)–(8):

$$\delta^{202}Hg_{sed.} = F_{cal.} \times \delta^{202}Hg_{cal.} + F_{ore} \times \delta^{202}Hg_{ore.} + F_{nat} \times \delta^{202}Hg_{nat.} \quad (6)$$

$$1/HgT_{sed.} = F_{cal.}/HgT_{cal.} + F_{ore}/HgT_{ore} + F_{nat}/HgT_{nat.} \quad (7)$$

$$1 = F_{cal.} + F_{ore} + F_{nat} \quad (8)$$

where subscripts cal., ore. and nat. refer to the Hg calcine origin, unroasted Hg ore origin and natural background origin, respectively; F$_{cal}$, F$_{ore}$ and F$_{nat.}$ represent the fraction of Hg originating from Hg calcine origin, unroasted Hg ore origin and natural background origin, respectively. Similarly, δ^{202}Hg$_{sed.}$ and HgT$_{sed.}$ refer to the δ^{202}Hg and HgT contents of the DSX downstream sediment, respectively. The definition of the three end members in the equation sets (Eqs. 6–8) are natural background origin (1/HgT$_{nat.}$, δ^{202}Hg$_{nat.}$), Hg calcine origin (1/HgT$_{cal.}$, δ^{202}Hg$_{cal.}$), and unroasted Hg ore origin (1/HgT$_{ore.}$, δ^{202}Hg$_{ore.}$), respectively. We assigned the HgT data of the background areas in WSMM (0.72 ± 0.44 μg g^{-1}, 2ό, n = 6) reported by Qiu et al. (2005) and the isotope composition of S13 and S14 to represent the
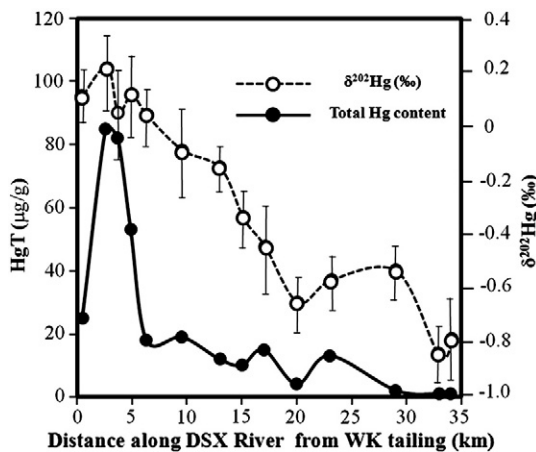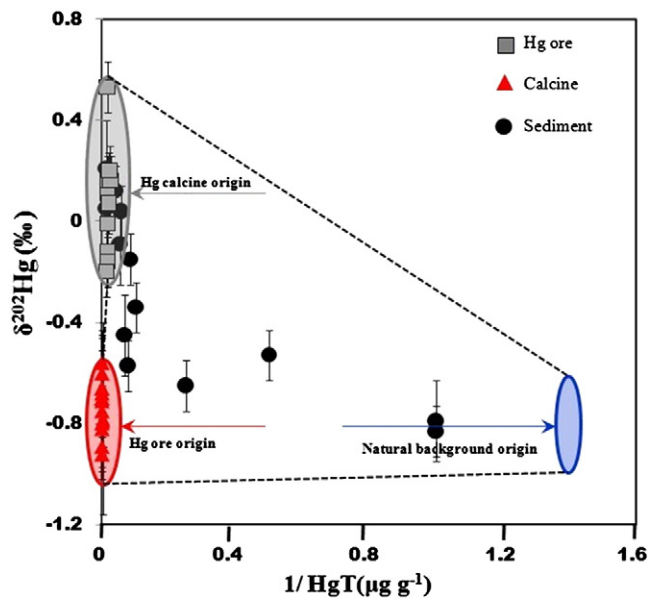
Fig. 6. Plot of δ^{202}Hg (‰) vs and 1/HgT (μg g^{-1}) in unroasted Hg ores, Hg wasted calcines and sediment samples.

natural background Hg end member (1/HgT$_{nat}$.: 1.39, δ^{202}Hg$_{nat}$.: -0.81%). The calcine Hg end member (1/HgT$_{cal}$.: 0.18, δ^{202}Hg$_{cal}$.: $+0.08\%$) and unroasted Hg ore origin (1/HgT$_{ore}$.: ~0, δ^{202}Hg$_{ore}$.: -0.74%) are defined using the mean HgT and mean δ^{202}Hg values of Hg calcines and unroasted Hg ore samples.

Based on Eqs. (6)–(8), the relative importance of the three sources was estimated and shown in Fig. 7. Our study suggested that the source attribution in DSX sediment can be divided into three segments. As shown in Fig. 7, within 17 km from the WK tailing, the dominant source in the sediment is of Hg calcine origin (>50%). In sediments collected from 17 to 30 km, the dominant source in the sediment is of unroasted Hg ore origin. In sediment more than 30 km away from the tailing, the Hg mainly originated from a natural geogenic source. In previous studies, quantification of Hg sources in sediments has been well developed by using simple MDF binary mixing models using Hg isotopes (Foucher et al., 2009). Furthermore, Liu et al. (2011) used a combined MDF/MIF triple mixing model to
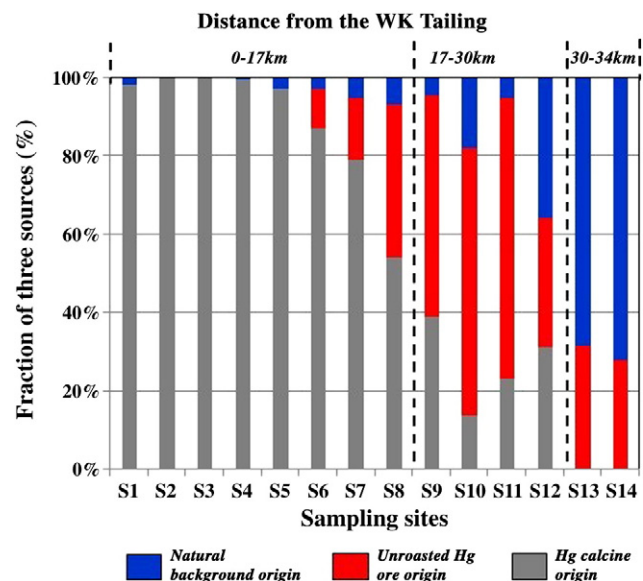
estimate the source attribution in the sediment from Dongjiang River, China. In this study, we demonstrated that the combined 1/HgT and MDF approach is a potentially useful tool to quantify the sources of Hg contamination to the sediment.

4. Conclusions

An EXAFS study was used to determine the Hg species and relative fractions of these species presented in unroasted Hg ore and Hg calcine in WSMM. The EXAFS result shows that the dominating Hg species in unroasted Hg ore is α-HgS, while the dominating components in mine waste calcine are β-HgS, α-HgS and HgCl$_2$. We suggested that the re-constructive phase transformation of α-HgS to other Hg by-products occurred (e.g. β-HgS and HgCl$_2$) during the calcining process.

The Hg isotopic analysis indicates that the unroasted Hg ore at WSMM has an isotopically narrow range of δ^{202}Hg composition of $-0.74 \pm 0.11\%$ (2$\acute{o}$, n = 13). However, the calcines (0.08 $\pm$ 0.20‰, 2$\acute{o}$, n = 13) have an isotopically heavier composition than the original ore materials, recording an Hg isotopic fractionation of ~0.82‰ in δ^{202}Hg values during the Hg ore roasting process. We interpreted that the heavier δ^{202}Hg in calcine samples resulted from the presence of Hg by-products, such as β-HgS and HgCl$_2$.

The variation of δ^{202}Hg appears to be large enough to distinguish between different contamination sources in the downstream sediment in WSMM. Following a binary mixing model, the relative fractions of three sources (i.e., calcine origin, Hg ore origin and natural background origin) in the DSX downstream sediment were also estimated. According to the model output, anthropogenic sources of Hg are predicted to yield an Hg contamination in the DSX sediment within a distance of 30 km from the headwater. Hence, Hg isotope can be a useful tool to direct the rehabilitation process in the WSMM area in the future.

References

Bergquist, B.A., Blum, J.D., 2007. Mass-dependent and -independent fractionation of Hg isotopes by photoreduction in aquatic systems. Science 318, 19.
Bergquist, B.A., Ghosh, S., Chanden, P., Rose, C., Blum, J.D., 2011. The exploration of the signatures of mass-independent fractionation of mercury. 10th International Conference of Mercury as a Global Pollutant. MG2-O3.
Biswas, A., Blum, J.D., Bergquist, B.A., Keeler, G.J., Xie, Z.Q., 2008. Natural mercury isotope variation in coal deposits and organic soils. Environmental Science and Technology 42, 8303–8309.
Blum, J.D., Bergquist, B.A., 2007. Reporting of variations in the natural isotopic composition of mercury. Analytical and Bioanalytical Chemistry 388, 353–359.
Chen, D.F., Sun, S.Q., 1991. Metacinnabar and tiemannite in Hunan–Guizhou (Xiangqian) mercury metallogenic belt. Acta Petrologica et Mineralogica 10 (1), 58–62.
Estrade, N., Carignan, J., Sonke, J.E., Donard, O.F.X., 2009. Mercury isotope fractionation during liquid–vapor evaporation experiments. Geochimica et Cosmochimica Acta 73, 2693–2711.
Feng, X.B., Qiu, G.L., 2008. Mercury pollution in Guizhou, Southwestern China — an overview. The Science of the Total Environment 400 (1–3), 227–237.
Feng, X.B., Li, P., Qiu, G.L., Wang, S.F., Li, G.H., Shang, L.H., Meng, B., Jiang, H.M., Bai, W.Y., Li, Z.G., Fu, X.W., 2008. Human exposure to methylmercury through rice intake in mercury mining areas, Guizhou province, China. Environmental Science and Technology 42, 326–332.
Feng, X.B., Foucher, D., Hintelmann, H., Yan, H.Y., He, T.R., Qiu, G.L., 2010. Tracing mercury contamination sources in sediments using mercury isotope compositions. Environmental Science and Technology 44, 3363–3368.
Foucher, D., Hintelmann, H., 2006. High-precision measurement of mercury isotope ratios in sediments using cold-vapor generation multi-collector inductively coupled plasma mass spectrometry. Analytical and Bioanalytical Chemistry 384, 1470–1478.
Foucher, D., Ogring, N., Hintelmann, H., 2009. Tracing mercury contamination from the Idrija mining region (Slovenia) to the Gulf of Trieste using Hg isotope ratio measurements. Environmental Science and Technology 43, 33–39.

Fig. 7. Fractions of three sources of Hg in sediment samples collected from the DSX River.

Gehrke, G.E., Blum, J.D., Meyers, P.A., 2009. The geochemical behavior and isotopic composition of Hg in a mid-Pleistocene western Mediterranean sapropel. Geochimica et Cosmochimica Acta 73, 1651–1665.

Gehrke, G.E., Blum, J.D., Marvin-DiPasquale, M., 2011. Sources of mercury to San Francisco Bay surface sediment as revealed by mercury stable isotopes. Geochimica et Cosmochimica Acta 75 (3), 691–705.

Gray, J.E., Theodorakos, P.M., Bailey, E.A., Turner, R.R., 2000. Distribution, speciation, and transport of mercury in stream-sediment, stream-water, and fish collected near abandoned mercury mines in southwestern Alaska, USA. The Science of the Total Environment 260, 21–33.

Gray, J.E., Hines, M.E., Biester, H., 2006. Mercury methylation influenced by areas of past mercury mining in the Terlingua district, Southwest Texas, USA. Applied Geochemistry 21, 1940–1954.

Hintelmann, H., Lu, S.Y., 2003. High precision isotope ratio measurements of mercury isotopes in cinnabar ores using multi-collector inductively coupled plasma mass spectrometry. Analyst 128, 635–639.

Horvat, M., Nolde, N., Fajon, V., Jereb, V., Logar, M., Lojen, S., Jacimovic, R., Falnoga, I., Liya, Q., Faganeli, J., Drobne, D., 2003. Total mercury, methylmercury and selenium in mercury polluted areas in the province Guizhou, China. The Science of the Total Environment 304, 231–256.

Hua, Y., Cui, M., 1994. Guizhou Wanshan Mercury Deposit. China Geological Press, Beijing. (in Chinese).

Huggins, F.G., Shah, N., Huffman, G.P., Robertson, J.D., 2000. XAFS spectroscopic characterization of elements in combustion ash and fine particulate matter. Fuel Processing Technology 65–66, 203–218.

Jackson, T.A., Whittle, D.M., Evans, M.S., Muir, D.G., 2008. Evidence for mass-independent and mass-dependent fractionation of the stable isotopes of mercury by natural processes in aquatic ecosystems. Applied Geochemistry 23, 547–571.

Kim, C.S., Brown Jr., G.E., Rytuba, J.J., 2000. Characterization and speciation of mercury-bearing mine wastes using X ray absorption spectroscopy (XAS). Science of the Total Environment 261, 157–168.

Kim, C.S., Rytuba, J.J., Brown Jr., J.E., 2004. Geological and anthropogenic factors influencing mercury speciation in mine wastes: an EXAFS spectroscopy study. Applied Geochemistry 19 (3), 379–393.

Koster van Groos, P.G., Esser, B.K., Williams, R., Hunt, J.R., 2007. Identifying environmental sources of mercury using stable mercury isotopes. Goldschmidt Conference Abstracts. A516.

Kritee, K., Blum, J.D., Johnson, M.W., Bergquist, B.A., Barkay, T., 2007. Mercury stable isotope fractionation during reduction of Hg(II) to Hg(0) by mercury resistant microorganisms. Environmental Science and Technology 41, 1889–1895.

Kritee, K., Blum, J.D., Barkay, T., 2008. Mercury stable isotope fractionation during reduction of Hg(II) by different microbial pathways. Environmental Science and Technology 42, 9171–9177.

Kullerud, G., 1965. The mercury–sulfur system. Carnegie I., 64, pp. 194–195.

Laffont, L., Sonke, J.E., Maurice, L., Hintelmann, H., Pouilly, M., Bacarreza, Y.S., Perez, T., Behra, P., 2009. Anomalous mercury isotopic compositions of fish and human hair in the Bolivian Amazon. Environmental Science and Technology 43, 8985–8990.

Lefticariu, L., Blum, J., Gleason, J., 2011. Mercury isotopic evidence for multiple mercury sources in coal from the Illinois Basin. Environmental Science and Technology 45 (4), 1724–1729.

Liu, J., Feng, X., Yin, R., Zhu, W., Li, Z., 2011. Mercury distributions and mercury isotope signatures in sediments of Dongjiang River, the Pearl River Delta, China. Chemical Geology, http://dx.doi.org/10.1016/j.chemgeo.2011.06.001.

Luis, R., Jesusa, R., Isaac, A., Laura, R.C., 2007. Capability of selected crop plants for shoot mercury accumulation from polluted soils: phytoremediation perspectives. International Journal of Phytoremediation 9, 1–13.

Lv, J., Luo, L., Zhang, J., Christie, P., Zhang, S., 2012. Adsorption of mercury on lignin: combined surface complexation modeling and X-ray absorption spectroscopy studies. Environmental Pollution 162, 255–261.

Mattielli, N., Petit, J., Deboudt, K., Flament, P., Perdrix, E., Taillez, A., Rimetz-Planchon, J., Weis, D., 2009. Zn isotope study of atmospheric emissions and dry depositions within a 5 km radius of a Pb–Zn refinery. Atmospheric Environment 43, 1265–1272.

National Research Council (NRC), 2000. Toxicological Effects of MeHg, Committee Report, Board of Environmental Studies and Toxicology. National Academy Press, Washing DC, p. 344.

Newville, M., 2001. IFEFFIT: interactive XAFS analysis and FEFF fitting. Journal of Synchrotron Radiation 8, 322–324.

Perrot, V., Epov, V.N., Pastukhov, M.V., Grebenshchikova, V.I., Zouiten, C., Sonke, J.E., Donard, O.F.X., Amouroux, D., 2010. Tracing sources and bioaccumulation of mercury in fish of Lake Baikal–Angara River using Hg isotopic composition. Environmental Science and Technology 44 (21), 8030–8037.

Qiu, G.L., Feng, X.B., Wang, S.F., Shang, L.H., 2005. Mercury and methylmercury in riparian soil, sediments, mine-waste calcines, and moss from abandoned Hg mines in east Guizhou province, southwestern China. Applied Geochemistry 20 (3), 627–638.

Qiu, G., Feng, X., Li, P., Wang, S., Li, G., Shang, L., Fu, X., 2008. Methylmercury accumulation in rice (Oryza sativa L.) grown at abandoned mines in Guizhou, China. Journal of Agriculture and Food Chemistry 56, 2465–2468.

Ressler, T., 1998. WinXAS: a program for X-ray absorption spectroscopy data analysis under MS-Windows. Journal of Synchrotron Radiation 5, 118–122.

Schauble, E.A., 2007. Role of nuclear volume in driving equilibrium isotope fractionation of mercury, thallium, and other very heavy elements. Geochimica et Cosmochimica Acta 71, 2170–2189.

Schroeder, W.H., Munthe, J., 1998. Atmospheric mercury — an overview. Atmospheric Environment 32, 809–822.

Sherman, L.S., Blum, J.D., Nordstrom, D.K., McCleskey, R.B., Barkay, T., Vetriani, C., 2009. Mercury isotopic composition of hydrothermal systems in the Yellowstone Plateau volcanic field and Guaymas Basin sea-floor rift. Earth and Planetary Science Letters 29, 86–96.

Smith, C.N., Kesler, S.E., Klaue, B., Blum, J.D., 2005. Mercury isotope fractionation in fossil hydrothermal systems. Geology 33, 825–828.

Smith, C.N., Keslera, S.E., Blum, J.D., Rytuba, J.J., 2008. Isotope geochemistry of mercury in source rocks, mineral deposits and spring deposits of the California Coast Ranges, USA. Earth and Planetary Science Letters 269, 399–407.

Sonke, J., Sivry, Y., Viers, J., Freydier, R., Dejonghe, L., André, L., Aggarwal, J., Fontan, F., Dupré, B., 2008. Historical variations in the isotopic composition of atmospheric zinc deposition from a zinc smelter. Chemical Geology 252, 145–157.

Sonke, J.E., Schafer, J., Chmeleff, J., Audry, S., Blanc, G., Dupre, B., 2010. Sedimentary mercury stable isotope records of atmospheric and riverine pollution from two major European heavy metal refineries. Chemical Geology 279 (3–4), 90–100.

Stetson, S.J., Gray, J.E., Wanty, R.B., Macalady, D.L., 2009. Isotopic variability of mercury in ore, mine-waste calcine, and leachates of mine-waste calcine from areas mined for mercury. Environmental Science and Technology 43 (19), 7331–7336.

SWSNANE, 2003. Specifications for Wolfram, Stannum, Mercury and Antimony Mineral Exploration DZ/T 0201—2002.

Yang, L., Sturgeon, R.E., 2009. Isotopic fractionation of mercury induced by reduction and ethylation. Analytical and Bioanalytical Chemistry 393, 377–385.

Yin, R., Feng, X., Shi, W., 2010a. Application of the stable-isotope system to the study of sources and fate of Hg in the environment: a review. Applied Geochemistry 25, 1467–1477.

Yin, R.S., Feng, X.B., Foucher, D., Shi, W.F., Zhao, Z.Q., Wang, J., 2010b. High precision determination of mercury isotope ratios using online mercury vapor generation system coupled with multicollector inductively coupled plasma-mass spectrometer. Chinese Journal of Analytical Chemistry 38 (7), 929–934.

Zambardi, T., Sonke, J.E., Toutain, J.P., Sortino, F., Shinohara, H., 2009. Mercury emissions and stable isotopic compositions at Vulcano Island (Italy). Earth and Planetary Science Letters 277, 236–243.

Zhang, G.P., Liu, C.Q., Wu, P., Yang, Y.G., 2004. The geochemical characteristics of mine-waste calcines and runoff from the Wanshan mercury mine, Guizhou, China. Applied Geochemistry 19, 1735–1744.

Zhang, H., Feng, X.B., Thorjørn, L., Shang, L.H., Vogt, R.D., Rothenberg, S.E., Li, P., Zhang, H., Lin, Y., 2010. Fractionation, distribution and transport of mercury in rivers and tributaries around Wanshan Hg mining district, Guizhou Province, Southwestern China: part 1 total mercury. Applied Geochemistry 25, 633–641.

Zhao, T.C., Wang, J., 1999. A Handbook for Extractive Metallurgy of Nonferrous Metals. Metallurgical Industry Press. (In Chinese).

Zheng, W., Hintelmann, H., 2009. Mercury isotope fractionation during photoreduction in natural water is controlled by its Hg/DOC ratio. Geochimica et Cosmochimica Acta 73, 6704–6715.

Zheng, W., Foucher, D., Hintelmann, H., 2007. Mercury isotope fractionation during volatilization of Hg(0) from solution into the gas phase. Journal of Analytical Atomic Spectrometry 22, 1097–1104.